

Multi-spectrum retrieval of Venus IR surface emissivity maps from VIRTIS/VEX nightside measurements at Themis Regio - Supplementary material -

David Kappel^{a,b,*}, Gabriele Arnold^a, Rainer Haus^c

^aGerman Aerospace Center (DLR), Institute of Planetary Research, Rutherfordstrasse 2, 12489 Berlin, Germany

^bUniversity of Potsdam, Institute of Physics and Astronomy, Karl-Liebknecht-Straße 24/25, 14476 Potsdam-Golm, Germany

^cWestfälische Wilhelms-Universität Münster, Institute for Planetology, Wilhelm-Klemm-Straße 10, 48149 Münster, Germany

Abstract

The spectrally resolved VIRTIS-M-IR images utilized for this work (Kappel et al., 2016) are listed in Appendix A.1. Appendix A.2 presents the mathematical background of the renormalization. Detector-related trends of the VIRTIS-M-IR spectral registration retrieved from the measurements themselves are reported in Appendix A.3. Appendix A.4 shows figures that illustrate at 1.10 and 1.18 μm the post-processing of the retrieved maps and the MSTs and PMTs, complementing the corresponding figures at 1.02 μm given in the main text.

A. Appendix - Supplementary material

A.1. Utilized data cubes

This appendix lists the VIRTIS-M-IR spectrally resolved images ('data cubes') utilized for this work. Each Venus Express orbit corresponds to 24 (Earth-)hours (when VIRTIS-M-IR still acquired data). VIRTIS-M-IR data from each orbit are divided into a number of sessions, depending on the science objectives. For each VIRTIS-M-IR cube name, the number preceding the underscore denotes the orbit number, the number succeeding the underscore denotes the session. Each cube comprises a spectrally resolved (432 spectral bands uniformly dividing the approximate range 1.02–5.1 μm) two-dimensional spatial image (here only cubes used with 256 spatial samples and a number of spatial lines). The following 103 cubes contribute to the $N_r^0 = 64$ repetition data set. Note that the single cubes only partially cover the target area, and more than 64 cubes are needed, therefore, to achieve 64 repetitions for each surface bin.

108_00, 112_01, 121_01, 228_01, 229_01, 331_03, 331_04, 331_05, 332_01, 332_02, 332_03, 332_04, 332_05, 333_00, 333_01, 333_02, 333_03, 333_04, 333_05, 334_01, 342_00, 343_00, 344_00, 344_01, 344_02, 345_00, 345_01, 345_03, 347_00, 347_01, 347_03, 347_05, 349_01, 349_05, 351_01, 351_05, 359_02, 365_02, 365_05, 366_00, 366_01, 366_03, 366_04, 366_06, 366_07, 367_02, 367_05, 368_00, 368_01, 368_03, 368_04, 368_05, 368_07, 368_09, 368_11, 368_13, 368_15, 368_17, 368_19, 368_21, 368_23, 368_25, 368_27, 368_29, 368_31, 368_33, 368_35, 368_37, 368_39, 368_41, 368_43, 368_45, 368_47, 368_49, 368_51, 368_53, 368_55, 368_57, 368_59, 368_61, 368_63, 368_65, 368_67, 368_69, 368_71, 368_73, 368_75, 368_77, 368_79, 368_81, 368_83, 368_85, 368_87, 368_89, 368_91, 368_93, 368_95, 368_97, 368_99, 369_01, 369_03, 369_05, 369_07, 369_09, 369_11, 369_13, 369_15, 369_17, 369_19, 369_21, 369_23, 369_25, 369_27, 369_29, 369_31, 369_33, 369_35, 369_37, 369_39, 369_41, 369_43, 369_45, 369_47, 369_49, 369_51, 369_53, 369_55, 369_57, 369_59, 369_61, 369_63, 369_65, 369_67, 369_69, 369_71, 369_73, 369_75, 369_77, 369_79, 369_81, 369_83, 369_85, 369_87, 369_89, 369_91, 369_93, 369_95, 369_97, 369_99, 370_01, 370_03, 370_05, 370_07, 370_09, 370_11, 370_13, 370_15, 370_17, 370_19, 370_21, 370_23, 370_25, 370_27, 370_29, 370_31, 370_33, 370_35, 370_37, 370_39, 370_41, 370_43, 370_45, 370_47, 370_49, 370_51, 370_53, 370_55, 370_57, 370_59, 370_61, 370_63, 370_65, 370_67, 370_69, 370_71, 370_73, 370_75, 370_77, 370_79, 370_81, 370_83, 370_85, 370_87, 370_89, 370_91, 370_93, 370_95, 370_97, 370_99, 371_01, 371_03, 371_05, 371_07, 371_09, 371_11, 371_13, 371_15, 371_17, 371_19, 371_21, 371_23, 371_25, 371_27, 371_29, 371_31, 371_33, 371_35, 371_37, 371_39, 371_41, 371_43, 371_45, 371_47, 371_49, 371_51, 371_53, 371_55, 371_57, 371_59, 371_61, 371_63, 371_65, 371_67, 371_69, 371_71, 371_73, 371_75, 371_77, 371_79, 371_81, 371_83, 371_85, 371_87, 371_89, 371_91, 371_93, 371_95, 371_97, 371_99, 372_01, 372_03, 372_05, 372_07, 372_09, 372_11, 372_13, 372_15, 372_17, 372_19, 372_21, 372_23, 372_25, 372_27, 372_29, 372_31, 372_33, 372_35, 372_37, 372_39, 372_41, 372_43, 372_45, 372_47, 372_49, 372_51, 372_53, 372_55, 372_57, 372_59, 372_61, 372_63, 372_65, 372_67, 372_69, 372_71, 372_73, 372_75, 372_77, 372_79, 372_81, 372_83, 372_85, 372_87, 372_89, 372_91, 372_93, 372_95, 372_97, 372_99, 373_01, 373_03, 373_05, 373_07, 373_09, 373_11, 373_13, 373_15, 373_17, 373_19, 373_21, 373_23, 373_25, 373_27, 373_29, 373_31, 373_33, 373_35, 373_37, 373_39, 373_41, 373_43, 373_45, 373_47, 373_49, 373_51, 373_53, 373_55, 373_57, 373_59, 373_61, 373_63, 373_65, 373_67, 373_69, 373_71, 373_73, 373_75, 373_77, 373_79, 373_81, 373_83, 373_85, 373_87, 373_89, 373_91, 373_93, 373_95, 373_97, 373_99, 374_01, 374_03, 374_05, 374_07, 374_09, 374_11, 374_13, 374_15, 374_17, 374_19, 374_21, 374_23, 374_25, 374_27, 374_29, 374_31, 374_33, 374_35, 374_37, 374_39, 374_41, 374_43, 374_45, 374_47, 374_49, 374_51, 374_53, 374_55, 374_57, 374_59, 374_61, 374_63, 374_65, 374_67, 374_69, 374_71, 374_73, 374_75, 374_77, 374_79, 374_81, 374_83, 374_85, 374_87, 374_89, 374_91, 374_93, 374_95, 374_97, 374_99, 375_01, 375_03, 375_05, 375_07, 375_09, 375_11, 375_13, 375_15, 375_17, 375_19, 375_21, 375_23, 375_25, 375_27, 375_29, 375_31, 375_33, 375_35, 375_37, 375_39, 375_41, 375_43, 375_45, 375_47, 375_49, 375_51, 375_53, 375_55, 375_57, 375_59, 375_61, 375_63, 375_65, 375_67, 375_69, 375_71, 375_73, 375_75, 375_77, 375_79, 375_81, 375_83, 375_85, 375_87, 375_89, 375_91, 375_93, 375_95, 375_97, 375_99, 376_01, 376_03, 376_05, 376_07, 376_09, 376_11, 376_13, 376_15, 376_17, 376_19, 376_21, 376_23, 376_25, 376_27, 376_29, 376_31, 376_33, 376_35, 376_37, 376_39, 376_41, 376_43, 376_45, 376_47, 376_49, 376_51, 376_53, 376_55, 376_57, 376_59, 376_61, 376_63, 376_65, 376_67, 376_69, 376_71, 376_73, 376_75, 376_77, 376_79, 376_81, 376_83, 376_85, 376_87, 376_89, 376_91, 376_93, 376_95, 376_97, 376_99, 377_01, 377_03, 377_05, 377_07, 377_09, 377_11, 377_13, 377_15, 377_17, 377_19, 377_21, 377_23, 377_25, 377_27, 377_29, 377_31, 377_33, 377_35, 377_37, 377_39, 377_41, 377_43, 377_45, 377_47, 377_49, 377_51, 377_53, 377_55, 377_57, 377_59, 377_61, 377_63, 377_65, 377_67, 377_69, 377_71, 377_73, 377_75, 377_77, 377_79, 377_81, 377_83, 377_85, 377_87, 377_89, 377_91, 377_93, 377_95, 377_97, 377_99, 378_01, 378_03, 378_05, 378_07, 378_09, 378_11, 378_13, 378_15, 378_17, 378_19, 378_21, 378_23, 378_25, 378_27, 378_29, 378_31, 378_33, 378_35, 378_37, 378_39, 378_41, 378_43, 378_45, 378_47, 378_49, 378_51, 378_53, 378_55, 378_57, 378_59, 378_61, 378_63, 378_65, 378_67, 378_69, 378_71, 378_73, 378_75, 378_77, 378_79, 378_81, 378_83, 378_85, 378_87, 378_89, 378_91, 378_93, 378_95, 378_97, 378_99, 379_01, 379_03, 379_05, 379_07, 379_09, 379_11, 379_13, 379_15, 379_17, 379_19, 379_21, 379_23, 379_25, 379_27, 379_29, 379_31, 379_33, 379_35, 379_37, 379_39, 379_41, 379_43, 379_45, 379_47, 379_49, 379_51, 379_53, 379_55, 379_57, 379_59, 379_61, 379_63, 379_65, 379_67, 379_69, 379_71, 379_73, 379_75, 379_77, 379_79, 379_81, 379_83, 379_85, 379_87, 379_89, 379_91, 379_93, 379_95, 379_97, 379_99, 380_01, 380_03, 380_05, 380_07, 380_09, 380_11, 380_13, 380_15, 380_17, 380_19, 380_21, 380_23, 380_25, 380_27, 380_29, 380_31, 380_33, 380_35, 380_37, 380_39, 380_41, 380_43, 380_45, 380_47, 380_49, 380_51, 380_53, 380_55, 380_57, 380_59, 380_61, 380_63, 380_65, 380_67, 380_69, 380_71, 380_73, 380_75, 380_77, 380_79, 380_81, 380_83, 380_85, 380_87, 380_89, 380_91, 380_93, 380_95, 380_97, 380_99, 381_01, 381_03, 381_05, 381_07, 381_09, 381_11, 381_13, 381_15, 381_17, 381_19, 381_21, 381_23, 381_25, 381_27, 381_29, 381_31, 381_33, 381_35, 381_37, 381_39, 381_41, 381_43, 381_45, 381_47, 381_49, 381_51, 381_53, 381_55, 381_57, 381_59, 381_61, 381_63, 381_65, 381_67, 381_69, 381_71, 381_73, 381_75, 381_77, 381_79, 381_81, 381_83, 381_85, 381_87, 381_89, 381_91, 381_93, 381_95, 381_97, 381_99, 382_01, 382_03, 382_05, 382_07, 382_09, 382_11, 382_13, 382_15, 382_17, 382_19, 382_21, 382_23, 382_25, 382_27, 382_29, 382_31, 382_33, 382_35, 382_37, 382_39, 382_41, 382_43, 382_45, 382_47, 382_49, 382_51, 382_53, 382_55, 382_57, 382_59, 382_61, 382_63, 382_65, 382_67, 382_69, 382_71, 382_73, 382_75, 382_77, 382_79, 382_81, 382_83, 382_85, 382_87, 382_89, 382_91, 382_93, 382_95, 382_97, 382_99, 383_01, 383_03, 383_05, 383_07, 383_09, 383_11, 383_13, 383_15, 383_17, 383_19, 383_21, 383_23, 383_25, 383_27, 383_29, 383_31, 383_33, 383_35, 383_37, 383_39, 383_41, 383_43, 383_45, 383_47, 383_49, 383_51, 383_53, 383_55, 383_57, 383_59, 383_61, 383_63, 383_65, 383_67, 383_69, 383_71, 383_73, 383_75, 383_77, 383_79, 383_81, 383_83, 383_85, 383_87, 383_89, 383_91, 383_93, 383_95, 383_97, 383_99, 384_01, 384_03, 384_05, 384_07, 384_09, 384_11, 384_13, 384_15, 384_17, 384_19, 384_21, 384_23, 384_25, 384_27, 384_29, 384_31, 384_33, 384_35, 384_37, 384_39, 384_41, 384_43, 384_45, 384_47, 384_49, 384_51, 384_53, 384_55, 384_57, 384_59, 384_61, 384_63, 384_65, 384_67, 384_69, 384_71, 384_73, 384_75, 384_77, 384_79, 384_81, 384_83, 384_85, 384_87, 384_89, 384_91, 384_93, 384_95, 384_97, 384_99, 385_01, 385_03, 385_05, 385_07, 385_09, 385_11, 385_13, 385_15, 385_17, 385_19, 385_21, 385_23, 385_25, 385_27, 385_29, 385_31, 385_33, 385_35, 385_37, 385_39, 385_41, 385_43, 385_45, 385_47, 385_49, 385_51, 385_53, 385_55, 385_57, 385_59, 385_61, 385_63, 385_65, 385_67, 385_69, 385_71, 385_73, 385_75, 385_77, 385_79, 385_81, 385_83, 385_85, 385_87, 385_89, 385_91, 385_93, 385_95, 385_97, 385_99, 386_01, 386_03, 386_05, 386_07, 386_09, 386_11, 386_13, 386_15, 386_17, 386_19, 386_21, 386_23, 386_25, 386_27, 386_29, 386_31, 386_33, 386_35, 386_37, 386_39, 386_41, 386_43, 386_45, 386_47, 386_49, 386_51, 386_53, 386_55, 386_57, 386_59, 386_61, 386_63, 386_65, 386_67, 386_69, 386_71, 386_73, 386_75, 386_77, 386_79, 386_81, 386_83, 386_85, 386_87, 386_89, 386_91, 386_93, 386_95, 386_97, 386_99, 387_01, 387_03, 387_05, 387_07, 387_09, 387_11, 387_13, 387_15, 387_17, 387_19, 387_21, 387_23, 387_25, 387_27, 387_29, 387_31, 387_33, 387_35, 387_37, 387_39, 387_41, 387_43, 387_45, 387_47, 387_49, 387_51, 387_53, 387_55, 387_57, 387_59, 387_61, 387_63, 387_65, 387_67, 387_69, 387_71, 387_73, 387_75, 387_77, 387_79, 387_81, 387_83, 387_85, 387_87, 387_89, 387_91, 387_93, 387_95, 387_97, 387_99, 388_01, 388_03, 388_05, 388_07, 388_09, 388_11, 388_13, 388_15, 388_17, 388_19, 388_21, 388_23, 388_25, 388_27, 388_29, 388_31, 388_33, 388_35, 388_37, 388_39, 388_41, 388_43, 388_45, 388_47, 388_49, 388_51, 388_53, 388_55, 388_57, 388_59, 388_61, 388_63, 388_65, 388_67, 388_69, 388_71, 388_73, 388_75, 388_77, 388_79, 388_81, 388_83, 388_85, 388_87, 388_89, 388_91, 388_93, 388_95, 388_97, 388_99, 389_01, 389_03, 389_05, 389_07, 389_09, 389_11, 389_13, 389_15, 389_17, 389_19, 389_21, 389_23, 389_25, 389_27, 389_29, 389_31, 389_33, 389_35, 389_37, 389_39, 389_41, 389_43, 389_45, 389_47, 389_49, 389_51, 389_53, 389_55, 389_57, 389_59, 389_61, 389_63, 389_65, 389_67, 389_69, 389_71, 389_73, 389_75, 389_77, 389_79, 389_81, 389_83, 389_85, 389_87, 389_89, 389_91, 389_93, 389_95, 389_97, 389_99, 390_01, 390_03, 390_05, 390_07, 390_09, 390_11, 390_13, 390_15, 390_17, 390_19, 390_21, 390_23, 390_25, 390_27, 390_29, 390_31, 390_33, 390_35, 390_37, 390_39, 390_41, 390_43, 390_45, 390_47, 390_49, 390_51, 390_53, 390_55, 390_57, 390_59, 390_61, 390_63, 390_65, 390_67, 390_69, 390_71, 390_73, 390_75, 390_77, 390_79, 390_81, 390_83, 390_85, 390_87, 390_89, 390_91, 390_93, 390_95, 390_97, 390_99, 391_01, 391_03, 391_05, 391_07, 391_09, 391_11, 391_13, 391_15, 391_17, 391_19, 391_21, 391_23, 391_25, 391_27, 391_29, 391_31, 391_33, 391_35, 391_37, 391_39, 391_41, 391_43, 391_45, 391_47, 391_49, 391_51, 391_53, 391_55, 391_57, 391_59, 391_61, 391_63, 391_65, 391_67, 391_69, 391_71, 391_73, 391_75, 391_77, 391_79, 391_81, 391_83, 391_85, 391_87, 391_89, 391_91, 391_93, 391_95, 391_97, 391_99, 392_01, 392_03, 392_05, 392_07, 392_09, 392_11, 392_13, 392_15, 392_17, 392_19, 392_21, 392_23, 392_25, 392_27, 392_29, 392_31, 392_33, 392_35, 392_37, 392_39, 392_41, 392_43, 392_45, 392_47, 392_49, 392_51, 392_53, 392_55, 392_57, 392_59, 392_61, 392_63, 392_65, 392_67, 392_69, 392_71, 392_73, 392_75, 392_77, 392_79, 392_81, 392_83, 392_85, 392_87, 392_89, 392_91, 392_93, 392_95, 392_97, 392_99, 393_01, 393_03, 393_05, 393_07, 393_09, 393_11, 393_13, 393_15, 393_17, 393_19, 393_21, 393_23, 393_25, 393_27, 393_29, 393_31, 393_33, 393_35, 393_37, 393_39, 393_41, 393_43, 393_45, 393_47, 393_49, 393_51, 393_53, 393_55, 393_57, 393_59, 393_61, 393_63, 393_65, 393_67, 393_69, 393_71, 393_73, 393_75, 393_77, 393_79, 393_81, 393_83, 393_85, 393_87, 393_89, 393_91, 393_93, 393_95, 393_97, 393_99, 394_01, 394_03, 394_05, 394_07, 394_09, 394_11, 394_13, 394_15, 394_17, 394_19, 394_21, 394_23, 394_25, 394_27, 394_29, 394_31, 394_33, 394_35, 394_37, 394_39, 394_41, 394_43, 394_45, 394_47, 394_49, 394_51, 394_53, 394_55, 394_57, 394_59, 394_61, 394_63, 394_65, 394_67, 394_69, 394_71, 394_73, 394_75, 394_77, 394_79, 394_81, 394_83, 394_85, 394_87, 394_89, 394_91, 394_93, 394_95, 394_97, 394_99, 395_01, 395_03, 395_05, 395_07, 395_09, 395_11, 395_13, 395_15, 395_17, 395_19, 395_21, 395_23, 395_25, 395_27, 395_29, 395_31, 395_33, 395_35, 395_37, 395_39, 395_41, 395_43, 395_45, 395_47, 395_49, 395_51, 395_53, 395_55, 395_57, 395_59, 395_61,

A.2. Mathematical model

This appendix clarifies the role of the renormalization and how it affects the retrieval errors. It motivates the error scaling properties (so far only assumed, see Section 4.1 and Kappel et al. (2015b)) and the underlying mechanisms of error origination. Certain simplifications are formulated that enable these discussions. Suitable comparison measures for results from different batches of the MSTs and for scenarios of the PMTs are defined.

A.2.1. Renormalization and variance

First of all, the removal of emissivity trends with latitude and topography (i.e. the 'de-trending') is introduced in terms of a linear operator. For this purpose, the raw retrieved emissivities from a given scenario and at a given wavelength index (that are momentarily not indicated here for simpler notation) are sorted into a column vector \mathbf{e}_M with entries $e_M(b)$, where $b \in \{1, \dots, B\}$ indicates the surface bin and the subscript M the emissivity mean value, $M = \sum_{b=1}^B e_M(b)/B$. The multiple linear regression model of \mathbf{e}_M with respect to latitudes $\boldsymbol{\theta}(b)$ (compiled into the vector $\boldsymbol{\theta}$) and surface elevations $\mathbf{h}(b)$ (forming the vector \mathbf{h}) can be written $\mathbf{e}_M = \beta^1 + \beta^2 \boldsymbol{\theta} + \beta^3 \mathbf{h} + \boldsymbol{\varepsilon}$, where $\boldsymbol{\varepsilon}$ is the vector of the residuals $\varepsilon(b)$ from the regression. The $\varepsilon(b)$ are later regarded as deviations of the de-trended emissivities from their emissivity mean value M , provided β^1 is such that $\sum_{b=1}^B \varepsilon(b) = 0$. Using the matrix $\mathbf{X} := (\mathbf{1}, \boldsymbol{\theta}, \mathbf{h})$ and the vector $\boldsymbol{\beta} := (\beta^1, \beta^2, \beta^3)^T$, this can be arranged into the equation $\mathbf{e}_M = \mathbf{X}\boldsymbol{\beta} + \boldsymbol{\varepsilon}$, where $\mathbf{1}$ is the B -dimensional column vector with all entries 1. The regression coefficients (β^1 is the intercept) can be found by minimizing the residual sum of squares $\boldsymbol{\varepsilon}^T \boldsymbol{\varepsilon} = (\mathbf{e}_M - \mathbf{X}\boldsymbol{\beta})^T (\mathbf{e}_M - \mathbf{X}\boldsymbol{\beta})$. The best estimate of $\boldsymbol{\beta}$ reads $\hat{\boldsymbol{\beta}} = (\mathbf{X}^T \mathbf{X})^{-1} \mathbf{X}^T \mathbf{e}_M$, which follows from zeroing the derivative of $\boldsymbol{\varepsilon}^T \boldsymbol{\varepsilon}$ with respect to $\boldsymbol{\beta}$. This gives rise to the 'residual matrix' $\mathbf{R} := \mathbf{1} - \mathbf{X}(\mathbf{X}^T \mathbf{X})^{-1} \mathbf{X}^T$ that allows for the computation of the residual of the regression $\hat{\boldsymbol{\varepsilon}} := \mathbf{e}_M - \mathbf{X}\hat{\boldsymbol{\beta}} = \mathbf{R}\mathbf{e}_M$, a vector with entries $\hat{\varepsilon}(b)$. It can be immediately verified that the linear operator \mathbf{R} is an orthogonal projector, i.e. $\mathbf{R}^2 = \mathbf{R}$ and $\mathbf{R}^T = \mathbf{R}$, and that $\mathbf{R}\mathbf{X} = \mathbf{0}$. See also Hogben (2006, Section 52.4) for a summary of multiple linear regression using the residual matrix. It now follows that $\mathbf{X}^T \hat{\boldsymbol{\varepsilon}} = \mathbf{X}^T \mathbf{R}\mathbf{e}_M = (\mathbf{R}\mathbf{X})^T \mathbf{e}_M = \mathbf{0}$, which implies $\sum_{b=1}^B \hat{\varepsilon}(b) = 0$ (since first entry of vector $\mathbf{X}^T \hat{\boldsymbol{\varepsilon}}$ equals zero), and thus that the mean value of the residuals $\hat{\varepsilon}(b)$ over the bins is zero. The de-trended emissivities are therefore written as $\mathbf{r}_M(b) = (\mathbf{R}\mathbf{e}_M)(b) + M$, or short $\mathbf{R}\mathbf{e}_M(b) + M$. \mathbf{r}_M has the mean value M (as indicated by the subscript) and does not exhibit a trend with latitude and topography anymore. A de-trending of \mathbf{r}_M yields \mathbf{r}_M again, since \mathbf{R} is a projector. Note that de-trending does not introduce topography features for constant raw emissivity maps. Moreover, raw emissivity maps that are perfectly correlated with topography do not exhibit topography features after de-trending, since $\mathbf{R}\mathbf{X} = \mathbf{0}$.

As it was discussed in Section 2.3 and quantified in Section 4.5, the de-trended emissivities spatially fluctuate around their mean value M with a higher amplitude for cases with higher M . A linear transformation was given that refers a de-trended map \mathbf{r}_M to another, defined mean value called 'reference emissivity' e_{ref} , here mostly 0.5. In the appendix, this linear transformation shall be defined also for not de-trended maps \mathbf{e}_M . In the notation of Section 4.5, it can then be written $\mathbf{e}_{e_{\text{ref}}} = \lambda_{M \rightarrow e_{\text{ref}}} \cdot (\mathbf{e}_M - M) + e_{\text{ref}}$. Obviously, $\mathbf{e}_{e_{\text{ref}}}$ has the mean value e_{ref} . It is called the 'raw emissivity map referred to the reference emissivity e_{ref} '.

The de-trended emissivity map referred to e_{ref} can be written $\mathbf{r}_{e_{\text{ref}}} = \lambda_{M \rightarrow e_{\text{ref}}} \cdot (\mathbf{r}_M - M) + e_{\text{ref}}$. It has the mean value e_{ref} . Since \mathbf{R} is a projector, $\mathbf{r}_{e_{\text{ref}}}$ is indeed a de-trended map, because $\mathbf{R}\mathbf{r}_{e_{\text{ref}}} = \lambda_{M \rightarrow e_{\text{ref}}} \mathbf{R}\mathbf{r}_M = \lambda_{M \rightarrow e_{\text{ref}}} \mathbf{R}\mathbf{e}_M = \lambda_{M \rightarrow e_{\text{ref}}} (\mathbf{r}_M - M) = \mathbf{r}_{e_{\text{ref}}} - e_{\text{ref}}$. Moreover, de-trending and transforming to another reference emissivity can be interchanged, since $\mathbf{R}(\lambda_{M \rightarrow e_{\text{ref}}} (\mathbf{e}_M - M) + e_{\text{ref}}) + e_{\text{ref}} = \mathbf{r}_{e_{\text{ref}}}$. The vector $\mathbf{r}_{e_{\text{ref}}}$ is called the 'renormalized emissivity map referred to reference emissivity e_{ref} '. Note that an additional renormalization of renormalized emissivities has no effect. \mathbf{R} can act not only on emissivities but also on the parameters the emissivities depend on (it just acts by a matrix multiplication). To avoid an additional denotation, the results are also called 'renormalized' in the latter case, even if there is no referring to a reference emissivity involved.

In the following, e_{ref} is always 0.5, and all maps are referred to 0.5. The subscripts of $\mathbf{e}_{e_{\text{ref}}}$ and $\mathbf{r}_{e_{\text{ref}}}$ are dropped for convenience, such that $\mathbf{e}_{0.5} := \mathbf{e}$ and $\mathbf{r}_{0.5} := \mathbf{r}$, and a new subscript utilization can be employed. Now, the raw retrieved maps from retrieval scenario s (referred to the reference emissivity 0.5) are denoted by \mathbf{e}_s . The renormalized map reads $\mathbf{r}_s = \mathbf{R}\mathbf{e}_s + 0.5$, since de-trending and transforming to another reference emissivity can be interchanged. Each scenario is characterized by a selection of measurements that N_r times cover the specified surface target of B surface bins, the retrieval pipeline, assumptions on interfering forward model parameters, the choice of the initial emissivity, data calibration and preprocessing, etc. Note that \mathbf{R} does not depend on scenario s since \mathbf{X} does not. This neglects that the topography of a surface bin can slightly vary for the binned measurements as a result of motion blurring (Kappel

et al., 2012) and because it is a weighted average that respects the surface areas the unbinned measurements actually cover, which can differ for different measurement repetitions. This does not change results of the present discussion. It is also assumed that there are no uncertainties in latitude and topography of each bin, such that \mathbf{R} is the proper renormalization operator also for true emissivities. There are two cases ('Topo. 30/65 km') where \mathbf{h} indeed differs to allow for the exploration of topography uncertainties. They are excluded here and evaluated separately.

Statistical properties of a random variable X are often described in terms of mean value μ and standard deviation σ . Given only these characteristics, the probability distribution on \mathbb{R} (the real numbers) that has the least information content (i.e. requires no further parameters for description) is a Gaussian. Usage of the standard deviation has some disadvantages. Most importantly, it is not additive for uncorrelated random variables. This can be overcome by using the variance σ^2 for the characterization of a probability distribution. When μ and σ^2 are not known, they have to be estimated from S random samples x_s of the random variable X . Unbiased estimates of μ and σ^2 , respectively, are the sample mean value $\bar{x} := \sum_{s=1}^S x_s/S$ and the sample variance $\text{Var}^s[x_s] := \sum_{s=1}^S (x_s - \bar{x})^2/(S-1)$ (DeGroot and Schervish, 2012, Section 8.7). The denominator $S-1$ for $\text{Var}^s[x_s]$ is used instead of S , since the mean value is not known and has to be estimated itself. An estimate is unbiased when its statistical expectation value coincides with the true value, in this case when the averages of the \bar{x} and the $\text{Var}^s[x_s]$, respectively, computed from many repetitions with always S samples approach μ and σ^2 . Note that the sample standard deviation $\sqrt{\text{Var}^s[x_s]}$ is a biased estimate of σ (Shao, 2003, for a correction factor in case of Gaussians see Example 3.4). Therefore, only after averaging (over bins), variances are expressed as double standard deviations in percent of the reference emissivity, and then also scaled to $N_r = 64$ repetitions to enable direct comparison to results in Section 3. The variance of the sample mean \bar{x} is σ^2/S (DeGroot and Schervish, 2012, Theorem 6.2.3) and can be estimated by $\text{Var}^s[x_s]/S$. The standard deviation of $\text{Var}^s[x_s] - \sigma^2$ in case of Gaussians is $\sqrt{2/(S-1)}\sigma^2$ (DeGroot and Schervish, 2012, Eq. 8.7.8). When averaging over B repetitions of computing $\text{Var}^s[x_s]$ with different choices of samples (i.e. over B bins), the standard deviation of $(\sqrt{\langle \text{Var}^s[x_s] \rangle} - \sigma)(\sqrt{\langle \text{Var}^s[x_s] \rangle} + \sigma) \approx (\sqrt{\langle \text{Var}^s[x_s] \rangle} - \sigma) \cdot 2\sigma$ follows as $\sigma^2\sqrt{2}/\sqrt{BS-B}$, where the angular brackets denote the averaging over the B repetitions. The double standard deviation relative error for the estimate of σ by $\sqrt{\langle \text{Var}^s[x_s] \rangle}$ can thus be estimated as about $\Delta := \sqrt{2}/\sqrt{BS-B}$. Note that the inverse of the square root exists for $S \geq 2$. Finally, the variance of the sum of uncorrelated random variables is the sum of the variances (DeGroot and Schervish, 2012, Theorem 4.6.6), and $\text{Var}^s[\zeta x_s] = \zeta^2 \text{Var}^s[x_s]$ and $\text{Var}^s[x_s + a] = \text{Var}^s[x_s]$ for constants ζ and a .

A.2.2. First order model

Recall that at a given surface window, the retrieved emissivity map \mathbf{e}_s of the target is referred to the reference emissivity 0.5. The true emissivity map $\hat{\mathbf{e}}$ is also to be understood as being referred to 0.5 (according to the mentioned transformation). To enable the following analysis of the error sources and the approximate statistical scaling properties, a number of simplifications are required. At bin b , $\mathbf{e}_s(b)$ is written in terms of deviations from the true emissivity $\hat{\mathbf{e}}(b)$ that originate in the failure to exactly know the true quantities that led to the radiances recorded by VIRTIS-M-IR. The 'hat' accent is used in the following to indicate those true quantities.

$$\mathbf{e}_s(b) \approx \hat{\mathbf{e}}(b) + \sum_{k=1}^{N_r} \sum_{p=1}^{P_t} \frac{\partial \hat{\mathbf{e}}(b)}{\partial \hat{\mathbf{t}}_{s,k}^p(b)} (\mathbf{t}_{s,k}^p(b) - \hat{\mathbf{t}}_{s,k}^p(b)) + \sum_{p=1}^{P_l} \frac{\partial \hat{\mathbf{e}}(b)}{\partial \hat{\mathbf{l}}^p(b)} (\mathbf{l}_s^p(b) - \hat{\mathbf{l}}^p(b)) + \sum_{p=1}^{P_c} \frac{\partial \hat{\mathbf{e}}(b)}{\partial \hat{c}_s^p} (c_s^p - \hat{c}^p) \quad (\text{A.1})$$

The ' \approx ' shall indicate that only a first order model is used here, which also neglects the impacts of noise, subsidiary retrieval solutions, numerical repeatability under slightly altered conditions, etc. There are P_t parameters $\hat{\mathbf{t}}_{s,k}^p(b)$ like the cloud bottom altitude or H_2O abundance that can vary with time (and location), where k denotes, which value this parameter has at the k -th of the N_r repetitions that form scenario s . The P_l parameters $\hat{\mathbf{l}}^p(b)$ (e.g. parameterization of offset to true deep atmospheric temperature field) can only vary with location (and thus do not depend on k or s). The P_c parameters \hat{c}^p are spatially and temporally constant (e.g. continuum parameters, initial emissivity) and therefore do neither depend on bin b nor on k nor s . The corresponding parameters without 'hat' denote the values that are assumed during the forward model simulations. To allow for the exploration of responses to modifications of certain parameters in the frame of the PMTs, $\mathbf{l}_s^p(b)$ and c_s^p can also depend on s . The retrieved parameters except for the emissivities themselves are all assumed to attain their true values, such that only the interfering parameters are considered as error contributors in this first order model. Even though there exist spatial-temporal correlations between the true parameters, all statistical correlations whatsoever are assumed to be negligibly small for this appendix. The renormalized true t -parameters are assumed to be normally distributed around their renormalized assumed counterparts, with estimated

variances (either with respect to location or to time) that can be approximated by their underlying (long-term) variances that are assumed to not depend on time, location, or retrieval scenario s . Furthermore, underlying variances over time at fixed location and variances over space at fixed time shall coincide with the underlying variance over time and location of the respective parameter. Finally, the partial derivatives $\partial\widehat{e}(b)/\partial\widehat{\mathbf{t}}_{s,k}^p(b)$ etc. are approximated to not depend on the values the parameters attain and to coincide with the simulated emissivity derivatives (without 'hat'). They are thus written as $1/N_r \cdot \partial e/\partial t^p$, $\partial e/\partial l^p$, and $\partial e/\partial c^p$, respectively. Note that modification of $\mathbf{t}_{s,k}^p(b)$ at just the k -th of the N_r repetitions only slightly affects $\mathbf{e}_s(b)$ (notice absence of index k compared to $\mathbf{t}_{s,k}^p(b)$) and ever less so with increasing N_r , whereas modification of temporally constant parameters concerns all N_r repetitions and has a larger effect on $\mathbf{e}_s(b)$ in the same magnitude as a single-spectrum derivative. This can be described by the factor $1/N_r$ in front of $\partial e/\partial t^p$. Then Eq. (A.1) implies

$$\mathbf{R}\mathbf{e}_s(b) \approx \mathbf{R}\widehat{\mathbf{e}}(b) + \sum_{p=1}^{P_t} \frac{\partial e}{\partial t^p} \frac{1}{N_r} \sum_{k=1}^{N_r} \mathbf{R}(\mathbf{t}_{s,k}^p(b) - \widehat{\mathbf{t}}_{s,k}^p(b)). \quad (\text{A.2})$$

The c -terms vanish, since \mathbf{R} applied to the b -independent c -parameters yields zero. The only true and assumed l -parameters considered for the present analysis (topography uncertainties have been excluded for now) are spatially slowly varying with latitude, and the spatial extension of the target has been chosen to allow for a good approximation of this variation by a function linear with latitude, compare $l0$ -parameters in Table 4. Hence, they are nearly annihilated by \mathbf{R} , and the l -terms are not considered furthermore.

The main objective of this appendix is a statistical characterization of $\mathbf{r}_s(b) - \widehat{\mathbf{r}}(b)$, the deviation of the renormalized retrieved emissivities $\mathbf{r}_s(b) = \mathbf{R}\mathbf{e}_s(b) + 0.5$ from renormalized true emissivities $\widehat{\mathbf{r}}(b) := \mathbf{R}\widehat{\mathbf{e}}(b) + 0.5$, i.e. the renormalized emissivity retrieval errors. The variance of $\mathbf{r}_s(b) - \widehat{\mathbf{r}}(b)$ over the bins is estimated by $\text{Var}_b[\mathbf{r}_s(b) - \widehat{\mathbf{r}}(b)] = \text{Var}_b[\mathbf{R}\mathbf{e}_s(b) - \mathbf{R}\widehat{\mathbf{e}}(b)] = \sum_{b=1}^B (\mathbf{R}\mathbf{e}_s(b) - \mathbf{R}\widehat{\mathbf{e}}(b))^2/B$, since the mean over the bins of $\mathbf{R}\mathbf{e}_s(b) - \mathbf{R}\widehat{\mathbf{e}}(b)$ is exactly zero and does not need to be estimated (therefore not $B-1$ but B as denominator). Note that this corresponds to the square of $\text{RMSD}[\mathbf{r}_s, \widehat{\mathbf{r}}] := \sqrt{\sum_{b=1}^B (\mathbf{r}_s(b) - \widehat{\mathbf{r}}(b))^2/B}$, the root-mean-square-deviation (RMSD) between \mathbf{r}_s and $\widehat{\mathbf{r}}$. Then Eq. (A.2) implies

$$\begin{aligned} \text{Var}_b[\mathbf{r}_s(b) - \widehat{\mathbf{r}}(b)] &\approx \text{Var}_b \left[\sum_{p=1}^{P_t} \frac{\partial e}{\partial t^p} \frac{1}{N_r} \sum_{k=1}^{N_r} \mathbf{R}(\mathbf{t}_{s,k}^p(b) - \widehat{\mathbf{t}}_{s,k}^p(b)) \right] \\ &\approx \sum_{p=1}^{P_t} \left(\frac{\partial e}{\partial t^p} \right)^2 \frac{1}{N_r^2} \sum_{k=1}^{N_r} \text{Var}_b[\mathbf{R}(\mathbf{t}_{s,k}^p(b) - \widehat{\mathbf{t}}_{s,k}^p(b))] \approx \frac{1}{N_r} \sum_{p=1}^{P_t} \left(\frac{\partial e}{\partial t^p} \right)^2 \text{Var}[\mathbf{R}(\mathbf{t}^p - \widehat{\mathbf{t}}^p)]. \end{aligned} \quad (\text{A.3})$$

The second approximation is valid, because all statistical correlations between the parameters were assumed to be negligibly small. The last approximation applies, since $\text{Var}_b[\mathbf{R}(\mathbf{t}_{s,k}^p(b) - \widehat{\mathbf{t}}_{s,k}^p(b))] \approx \text{Var}[\mathbf{R}(\mathbf{t}^p - \widehat{\mathbf{t}}^p)]$, where Var in the last term indicates the underlying variance over time and location of the term in the square brackets. The latter was assumed to have variances that are independent of time and location, and variances over time and those over location were assumed to coincide with the variance over time and location.

Note that, according to Eq. (A.3), modifications of assumed t -parameters by a constant offset or by a trend with latitude and topography do not change the renormalized emissivity errors in this simplified model, except for impacts of noise, subsidiary solutions, numerical repeatability under slightly altered conditions, etc., compare for instance $T0$ -parameters in Table 4.

A.2.3. Measurement Selection Tests

Each MST utilizes of a series of S batches with indices $s \in \{1, \dots, S\}$ that all have the same N_r such that $SN_r = N_r^0 = 64$, which is the measurement repetition number of the data set used for the results in Section 3. The scatter of the renormalized emissivities $\mathbf{r}_s(b)$ over the different batches provides a measure of their uncertainty at N_r repetitions. In this section, this measure is determined and compared with results from Appendix A.2.2.

Focusing on a single surface bin center b and unindicated wavelength index, the $\mathbf{r}_s(b)$ are distributed according to a certain underlying probability distribution, here assumed to be the normal distribution. Mean value $\mathbf{r}(b)$ (the underlying renormalized emissivity) and variance $\mathbf{V}(b)$ (the accuracy achievable for the renormalized emissivity derived from one batch with N_r repetitions) of the underlying Gaussian are not known and have to be estimated from the $\mathbf{r}_s(b)$. The

latter can be regarded as (quasi-)random sample of size S of the underlying probability distribution. The sample mean is estimated as $\bar{\mathbf{r}}(b) := \sum_{s=1}^S \mathbf{r}_s(b)/S$, sample variance as $\bar{\mathbf{V}}(b) := \text{Var}^s[\mathbf{r}_s(b)] = \sum_{s=1}^S (\mathbf{r}_s(b) - \bar{\mathbf{r}}(b))^2/(S-1)$. Note that it can be checked for the retrieved MST results that $\bar{\mathbf{V}}(b)$ does not significantly change with b .

The average value of $\mathbf{V}(b)$ is denoted as V . $\langle \bar{\mathbf{V}} \rangle := \sum_{b=1}^B \bar{\mathbf{V}}(b)/B$ is an (unbiased) estimate of V . Note that overlining of variables is associated with operations that involve batch indices s , whereas angular brackets involve bins b . $\langle \bar{\mathbf{V}} \rangle$ can be written

$$\langle \bar{\mathbf{V}} \rangle = \frac{1}{B} \sum_{b=1}^B \frac{1}{S-1} \sum_{s=1}^S (\mathbf{R}\mathbf{e}_s(b) - \mathbf{R}\bar{\mathbf{e}}(b))^2 = \frac{1}{S-1} \sum_{s=1}^S D_s^2, \quad (\text{A.4})$$

where $\bar{\mathbf{e}}(b) = \sum_{s=1}^S \mathbf{e}_s(b)/S$, and $D_s := \text{RMSD}[\mathbf{r}_s, \bar{\mathbf{r}}] = \text{RMSD}[\mathbf{R}\mathbf{e}_s, \mathbf{R}\bar{\mathbf{e}}]$. This close link between $\langle \bar{\mathbf{V}} \rangle$ and the D_s suggests to use D_s to describe the dissimilarity of the renormalized emissivity maps \mathbf{r}_s determined from the different batches s (in particular when observing the structural similarity to the identity $\text{Var}_b[\mathbf{r}_s(b) - \hat{\mathbf{r}}(b)] = (\text{RMSD}[\mathbf{r}_s, \hat{\mathbf{r}}])^2$, see comment before Eq. (A.3), that measures the renormalized retrieval errors in terms of a root-mean-square-deviation). Observation of the D_s can be used to explore the variability of the retrieval results with respect to data selection. For a selection of MSTs (with given N_r), the D_s for each s and the three wavelength indices are listed in Table 4 in the columns SRMSD ('scaled' RMSD) in a scaled form, $2D_s/\sqrt{S-1}$ in percent of the reference emissivity 0.5. With denominator \sqrt{S} instead of $\sqrt{S-1}$, they would in a reasonable sense be scaled to $N_r = 64$ repetitions as will be seen. But at this point it seems more natural to use denominator $\sqrt{S-1}$, because then, the scaled D_s need only be quadratically averaged to obtain $2\sqrt{\langle \bar{\mathbf{V}} \rangle}/\sqrt{S}$ in percent of the reference emissivity, a value that will be shown below to estimate the percental double standard deviation error of the $N_r^0 = 64$ -map. This scaling of D_s therefore enables a direct comparison to the other error measures in this work. Note that the denominator $\sqrt{S-1}$ relatively increases the SRMSDs with small S (i.e. large N_r) with respect to those with large S (small N_r) in Table 4.

According to Eq. (A.2), $\langle \bar{\mathbf{V}} \rangle = \sum_{b=1}^B \text{Var}^s[\mathbf{R}\mathbf{e}_s(b)]/B$ can be approximated by

$$\langle \bar{\mathbf{V}} \rangle \approx \frac{1}{B} \sum_{b=1}^B \text{Var}^s \left[\sum_{p=1}^{P_t} \frac{\partial e}{\partial t^p} \frac{1}{N_r} \sum_{k=1}^{N_r} \mathbf{R}(\mathbf{t}_{s,k}^p(b) - \hat{\mathbf{t}}_{s,k}^p(b)) \right] \approx \frac{1}{B} \sum_{b=1}^B \sum_{p=1}^{P_t} \left(\frac{\partial e}{\partial t^p} \right)^2 \frac{1}{N_r^2} \sum_{k=1}^{N_r} \text{Var}^s[\mathbf{R}(\mathbf{t}_{s,k}^p(b) - \hat{\mathbf{t}}_{s,k}^p(b))],$$

because $\hat{\mathbf{e}}(b)$ is independent of batch s and hence a constant with respect to variance estimation over s , and all statistical correlations between the parameters were assumed to be negligibly small. In the same way as for Eq. (A.3), one has $\text{Var}^s[\mathbf{R}(\mathbf{t}_{s,k}^p(b) - \hat{\mathbf{t}}_{s,k}^p(b))] \approx \text{Var}[\mathbf{R}(\mathbf{t}^p - \hat{\mathbf{t}}^p)]$, which is independent of k and b . The averaging over bins can be omitted, therefore. Note that, to obtain a more stable statistics, this averaging is still performed when estimating $\langle \bar{\mathbf{V}} \rangle$ from the renormalized emissivity maps determined from the S batches. Finally, using Eq. (A.3),

$$\langle \bar{\mathbf{V}} \rangle = \frac{1}{B} \sum_{b=1}^B \text{Var}^s[\mathbf{r}_s(b)] \approx \frac{1}{N_r} \sum_{p=1}^{P_t} \left(\frac{\partial e}{\partial t^p} \right)^2 \text{Var}[\mathbf{R}(\mathbf{t}^p - \hat{\mathbf{t}}^p)] \approx \text{Var}_b[\mathbf{r}_{s_0}(b) - \hat{\mathbf{r}}(b)], \quad (\text{A.5})$$

which explicitly shows the independence of $\langle \bar{\mathbf{V}} \rangle$ from S (as it should be).

Hence, $\text{Var}_b[\mathbf{r}_{s_0}(b) - \hat{\mathbf{r}}(b)]$, the measure for the renormalized emissivity retrieval errors (at a given wavelength index) for a certain retrieval scenario s_0 with N_r repetitions, can be approximately estimated by $\langle \bar{\mathbf{V}} \rangle = \sum_{b=1}^B \text{Var}^s[\mathbf{r}_s(b)]/B$, the measure for the scatter and thus the statistical uncertainty (with respect to data selection but otherwise under the same scenario) of the renormalized emissivities determined from single batches with N_r repetitions. This is not too surprising, given the various simplifications that led to this result. But it can serve to discuss a number of important properties.

The error estimation for the results from Section 3 at $N_r^0 = 64$ repetitions cannot be directly performed by computing $\langle \bar{\mathbf{V}} \rangle$ with $N_r = 64$, since the N_r^0 retrieval run cannot be repeated using one or even several additional disjoint data sets due to lacking coverage of the target area with usable measurements as defined in Section 2.1. But the error scaling properties with N_r should be compatible with Eq. (A.5). This can be used to estimate the N_r^0 -error with an MST by dividing the N_r^0 data set into S disjoint sets (batches) that always cover the target $N_r^0/S = N_r^{\text{MST}}$ times and computing the corresponding $\langle \bar{\mathbf{V}} \rangle$. Taking the $(\partial e/\partial t^p)^2 \text{Var}[\mathbf{R}(\mathbf{t}^p - \hat{\mathbf{t}}^p)]$ to be unchanged, the error for N_r^0 (one standard deviation) can then be extrapolated as $\sqrt{\langle \bar{\mathbf{V}} \rangle} \cdot \sqrt{N_r^{\text{MST}}/N_r^0} = \sqrt{\langle \bar{\mathbf{V}} \rangle}/\sqrt{S}$. Since the $\bar{\mathbf{V}}(b)$ are averaged over

$B = 219 \gg 1$ bins (Section 2.1) before taking the square root, the standard deviation bias nearly vanishes even for $S = 2$. Note that the ‘sample standard deviation of the mean’ over all S batches, referred to $\bar{r}(b)$, is an intuitive scatter error estimation for the N_r^0 -result at b , because it is a measure for the scatter error of the average value over all S batches of the renormalized emissivities. It reads $\sqrt{\overline{V}(b)}/\sqrt{S}$, and the average over all bins (performed in terms of variances to avoid bias) results as $\sqrt{\langle \overline{V} \rangle}/\sqrt{S}$, which coincides with the extrapolated N_r^0 -error. To enable direct comparison to the other error measures in the present work, $\langle \overline{V} \rangle$ for an MST with N_r repetitions and S batches is represented in terms of double standard deviations referred to $N_r^0 = 64$ repetitions, $\delta^{N_r, S} := 2\sqrt{\langle \overline{V} \rangle}/\sqrt{S}$, in percent of the reference emissivity 0.5. This discussion also justifies the scaled form of the D_s from Eq. (A.4) as $2D_s/\sqrt{S}$ in percent of the reference emissivity, but recall that the denominator $\sqrt{S-1}$ is used for representation in Table 4 to enable a more direct comparison to N_r^0 . For the present work, $\delta^{32,2}$, $\delta^{16,4}$, and $\delta^{8,8}$ are determined (see Table 5), which will be used to estimate the uncertainty of the $N_r^0 = 64$ -maps shown in Fig. 3.

Retrospectively, Eq. (A.5) also justifies the assumed multi-spectrum retrieval error scaling rules proposed by Kappel et al. (2015b) (see Section 4.1 of the present work). Namely, of the considered parameters only t -parameters contribute in the first order to the double standard deviation renormalized emissivity retrieval errors, errors from different parameters are quadratically added (square root of sum of squares), and errors scale with $1/\sqrt{N_r}$ and correspond to single-spectrum retrieval errors for $N_r = 1$. It can now be clarified in which way the errors listed by these authors (determined from single-spectrum retrievals with synthetic spectra, summarized in Table 3 of the present work) are to be understood. They describe the spatially averaged scatter with respect to data selection and are only first order approximations under the condition of the various assumptions formulated in Appendix A.2.2. The first order contribution from a single parameter at $N_r = 1$ to the double standard deviation renormalized emissivity error is the derivative of the emissivity with respect to this parameter, multiplied by the expected double standard deviation of the renormalized parameter variation. This is the same as the first order emissivity variation resulting from a parameter change corresponding to the double standard deviation of the parameter. This is exactly the way, how errors were estimated by Kappel et al. (2015b). But note that some of the emissivity responses in that paper were already in the non-linear regime. The reasons for disagreements between errors listed there and in the present work lie in violations of the assumptions, in particular, the first order-assumption, the independence of the emissivity derivatives from the parameter values, insufficient assumptions on the expected ranges of the interfering parameters, the simplified correlation and variance properties, and the increased information content taken into account with multi-spectrum retrieval.

Eq. (A.5) also states that any errors on the parameter assumptions that are annihilated by \mathbf{R} have no first order impact on the renormalized emissivity maps. In particular, the renormalized emissivity maps are not affected when the spatial distribution of the long-term average of an interfering parameter (e.g. cloud bottom altitude) exhibits a slowly varying latitudinal trend that is not reflected in the assumed parameter values used in the retrievals. A constant offset does also not change the renormalized emissivity maps under the assumptions stated in Appendix A.2.2. In the same way, modifications to c -parameters (continua, initial emissivity) and latitudinal l -parameter trends (deep atmospheric temperature profile) have no impact. However, real-world responses to such parameter modifications are non-zero even for theoretically vanishing error contributions ($c0$ - and $l0$ -PMTs in Table 4; there are no $t0$ -parameters). This is due to higher order terms etc.

A.2.4. Parameter Modification Tests

The PMTs serve to study the impact of modifications to a number of assumed parameters and to characteristics of retrieval pipeline, calibration, and preprocessing on the renormalized emissivity maps. To save resources, the maps are determined from only $N_r = 25$ repetitions, and results are scaled to $N_r^0 = 64$. The base map \mathbf{r}_0 , with respect to which the modified maps \mathbf{r}_P are compared, is determined from scenario ‘ $N_r = 25$ base’ and denoted by the index ‘0’. The index ‘ P ’ runs through the other different bold-typed shortcuts used in the PMT descriptions in Section 4.4.

In analogy to the definition of D_s from Eq. (A.4), the dissimilarity of \mathbf{r}_P from \mathbf{r}_0 is measured as $D_{P,0} := \text{RMSD}[\mathbf{r}_P, \mathbf{r}_0] = \sqrt{\text{Var}_b[\mathbf{r}_P(b) - \mathbf{r}_0(b)]}$ (last equation in the same way as comment before Eq. (A.3)). Using Eq. (A.2), this leads to

$$(D_{P,0})^2 \approx \text{Var}_b \left[\frac{\partial e}{\partial t} \frac{1}{N_r} \sum_{k=1}^{N_r} \mathbf{R}(\mathbf{t}_{P,k}(b) - \mathbf{t}_{0,k}(b)) \right] \approx \frac{1}{N_r} \left(\frac{\partial e}{\partial t} \right)^2 \text{Var}[\mathbf{R}(\mathbf{t}_P - \mathbf{t}_0)], \quad (\text{A.6})$$

because $\mathbf{R}\hat{\mathbf{e}}(b)$ and the true parameters do not differ between a PMT and the ‘ $N_r = 25$ base’-case. Since only one

parameter is modified between each 'P'- and the '0'-case, the superscript '^p' is omitted for the t -variables. (Again, none of the considered c - or l -parameters contributes, since their differences between the 'P'- and the '0'-case are annihilated by \mathbf{R} .) Regarding the second approximation, note that the considered assumed t -parameters are either 'under control', because they are set to constant values and have really the character of l - or c -parameters (like cloud parameters, minor gases). Or, the difference between the 'P'- and '0'-parameters statistically varies in the same way as for a true parameter (e.g. difference of residuals from different straylight removal procedures). Hence, the second approximation applies, in the former case trivially so, because the parameters are annihilated by \mathbf{R} , and in the second case for reasons analogous to those given for Eq. (A.3).

Eq. (A.6) states that any modifications to the parameter assumptions that are annihilated by \mathbf{R} have no impact on the renormalized emissivity maps. But corresponding real-world responses are non-zero even for theoretically vanishing error contributions ($c0$ - and $l0$ -PMTs in Table 4). This is due to higher order terms and other assumptions that do not fully apply. For each PMT and the three wavelength indices, the $D_{P,0}$ are listed in Table 4 in the columns SRMSD in a scaled form, $D_{P,0} \cdot F$ in percent of the reference emissivity 0.5. The scaling factor F is set to $\sqrt{25/64}$ for t -parameters ('t' on the right in the 'Scenario'-column) and to 1 elsewhere. The former cases profit from an increase of N_r due to an averaging-out effect, because at fixed bin they statistically vary with time, see Eq. (A.6), the latter not. This way, the $D_{P,0}$ are in a reasonable sense scaled to $N_r^0 = 64$ repetitions. Note that they are already without a factor of 2 comparable (see Eq. (A.6) for t -parameters) to percental double standard deviation errors by way of the choice of their perturbations' magnitudes as expected double standard deviations, compare Kappel et al. (2015b, Table 1).

Parameter modifications (in the way of the PMTs) to the N_r^0 -case itself lead to additional errors to the MST error estimate for the N_r^0 -map. This impact cannot be directly determined due to the huge computational resources this would require. To still obtain a rough estimate of this effect, the squared PMT errors $(D_{P,0})^2$ are scaled to N_r^0 repetitions (then denoted as $(D_{P',s_0})^2$) and added to the squared MST error estimate $\text{Var}_b[\mathbf{r}_{s_0}(b) - \hat{\mathbf{r}}(b)]$. This can be motivated by

$$\text{Var}_b[\mathbf{r}_{P'}(b) - \hat{\mathbf{r}}(b)] = \text{Var}_b[\mathbf{r}_{s_0}(b) - \hat{\mathbf{r}}(b) + \mathbf{r}_{P'}(b) - \mathbf{r}_{s_0}(b)] = \text{Var}_b[\mathbf{r}_{s_0}(b) - \hat{\mathbf{r}}(b)] + (D_{P',s_0})^2 + \xi, \quad (\text{A.7})$$

with the covariance $\xi = 2 \text{Cov}_b[\mathbf{r}_{s_0}(b) - \hat{\mathbf{r}}(b), \mathbf{r}_{P'}(b) - \mathbf{r}_{s_0}(b)]$ (DeGroot and Schervish, 2012, Theorem 4.6.6). \mathbf{r}_{s_0} is the renormalized retrieved emissivity map for the N_r^0 -case and $\mathbf{r}_{P'}$ the result from a hypothetical PMT at N_r^0 repetitions. ξ is possibly not negligible, but it should be small compared to the other terms on the right hand side of Eq. (A.7). Note that it is theoretically (according to Eq. (A.6)) zero for the PMTs where the parameters are 'under control' as above, since the square of the covariance does not exceed the product of the variances of its two input variables (DeGroot and Schervish, 2012, Theorem 4.6.3). Some of the PMTs study the same parameter but in different ways (different initial emissivities, different deep atmospheric temperature field perturbations, etc.), other PMTs have been performed just for general interest (e.g. 'Surface haze', 'H₂SO₄ alt. gradient'). Thus, only the PMT errors indicated by '**' in the 'Scenario'-column of Table 4 are added to the MST error estimate, see Table 5.

A.3. Wavelength of first spectral band and spectral FWHM

This section gives additional retrieval results that are less relevant for the conclusions of the present paper but are still interesting on their own. It is discussed in Section 2.4 that there are parameters describing the spectral registration that are not sufficiently predictable by the current calibration pipeline and that are crucial for emissivity retrieval. The wavelength λ_1^s of the first spectral band and the full-width-at-half-maximum $FWHM^s$ of the spectral instrumental response function have to be retrieved from the spectra themselves as additional parameters. They are found to vary with spatial sample on the detector and detector temperature. Note that the other, not detector-related, retrieved parameters (clouds, gases) cover only a small part of the global latitude–longitude or latitude–local-time space, respectively, and are therefore less representative of any potential global trends.

The scatterplot in Fig. A.1 depicts this dependence for λ_1^s as retrieved from the ' $N_r^0 = 64$ ' data set comprising 14,016 spectra (after binning). Note that the detector sample in the figure is the average over the sample values of the VIRTIS-M-IR pixels contributing to the respective binned spectrum (see Section 2.1). There is a trend of lower λ_1^s with higher detector temperature (order of 0.8 nm/K). This trend is not strict indicating secondary dependencies on further parameters. For a fixed VIRTIS-M-IR frame (and hence at fixed temperature), λ_1^s tends to drop by about 1 nm from sample 1 at the left edge of the detector to about sample 100 where a local minimum occurs. It then rises by about 0.5 nm over the next 100 samples and roughly stays at this level up to sample 256 at the right edge. At average temperatures,

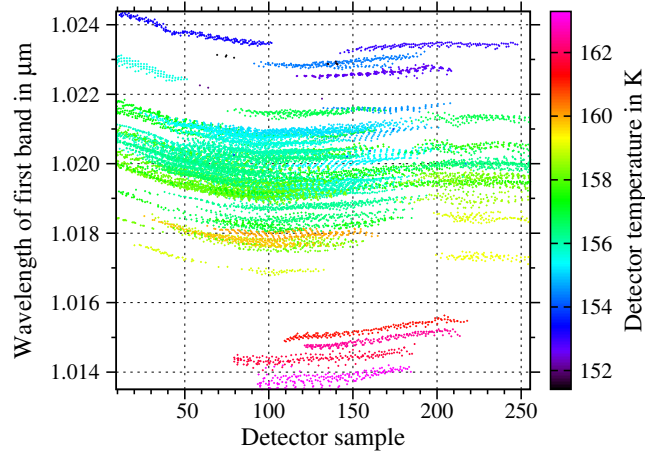


Figure A.1: Dependence of wavelength λ_1^s of first spectral band on detector sample and temperature.

1.020 μm is a representative value for λ_1^s at the detector center. Measurements at higher detector temperatures are better suited to sample the low-wavelength flank of the nightside surface window peak at 1.02 μm that is only partially covered by VIRTIS-M-IR.

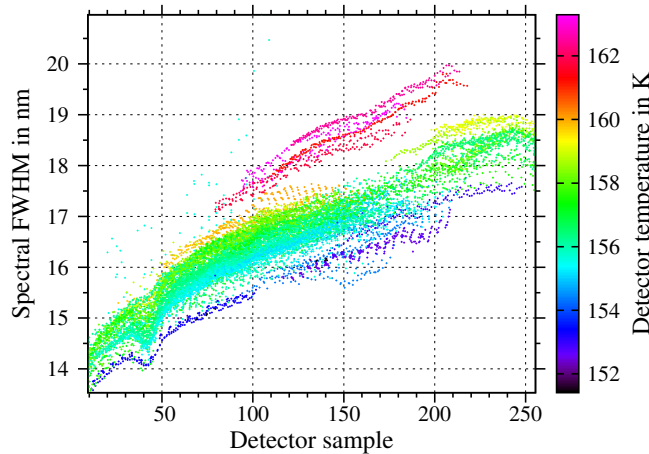


Figure A.2: Dependence of spectral FWHM on detector sample and temperature.

Fig. A.2 depicts the dependence of $FWHM^s$ as retrieved from the same measurement data set. This time, there is a (not strict) trend of higher $FWHM^s$ with higher detector temperature (order of 0.25 nm/K). For a fixed VIRTIS-M-IR frame, $FWHM^s$ tends to increase by about 4 nm from the left edge of the detector to the right edge. This increase is more pronounced for the 75 leftmost samples. At average temperatures, 17 nm is a representative value for $FWHM^s$ at the detector center. Measurements at lower detector temperatures and on the left part of the detector are better suited to resolve spectral features. Note that both λ_1^s and $FWHM^s$ are derived from the wavelength range 1.0–2.3 μm utilized for this work and may not be valid for the remaining VIRTIS-M-IR range up to 5.1 μm .

A.4. Additional figures

This section presents figures analogous to Figs. 1 and 4 but for the 1.10 and 1.18 μm surface windows instead of the 1.02 μm window.

Fig. A.3 illustrates the de-trending at 1.10 μm . The impact of the trend with topography is larger than at 1.02 μm . Also, the effect of the removal of the latitudinal trend is more pronounced than at 1.02 μm . In contrast, the trends at

1.18 μm are of a much smaller magnitude, see Fig. A.4. Recall that the transformation to the reference emissivity 0.5 still has to be performed in order to obtain Figs. 3b and c.

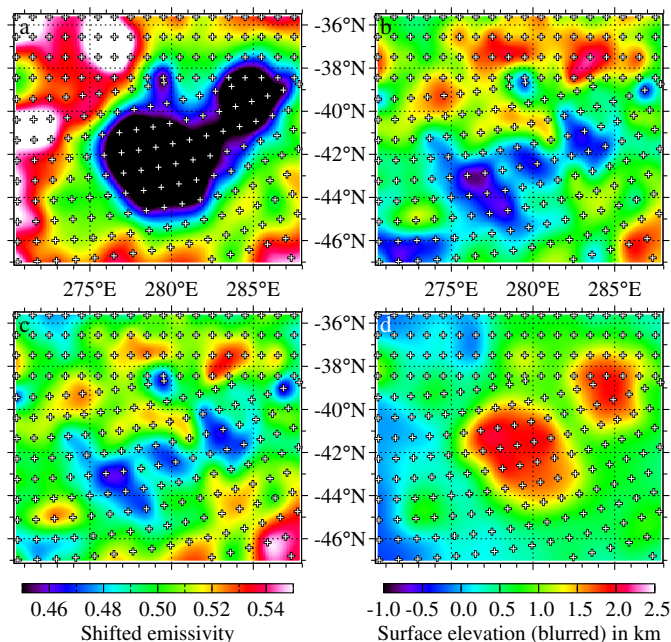


Figure A.3: Removal of trends with topography and latitude for the 1.10 μm emissivity map of Themis Regio retrieved from the $N_r^0 = 64$ measurement repetition data set. (a) Raw map, (b) trend with topography removed, (c) trends with topography and latitude removed, (d) utilized surface elevation (blurred Magellan topography). Representation as in Fig. 1.

One of the main results of this work is the estimate for the reliability of the renormalized emissivity maps. It was found that the double standard deviation uncertainties for the 1.02, 1.10, and 1.18 μm maps derived from 64 measurement repetitions are given by 3.3%, 8.4%, 4.0%, respectively, of the reference emissivity 0.5. Fig. A.5 illustrates that the 1.10 μm map is quite unreliable compared to the map at 1.02 μm . The PMT 'Continuum 1.74 μm ', which leads to almost the largest SRMSD contributing to the total error at 1.10 μm (see Table 4), still yields quite similar patterns between Figs. A.5c and d. However, the most direct and demonstrative test, the MST where maps are determined from two disjoint data sets, shows that the spatial patterns disagree between Figs. A.5a and b. This measurement repeatability failure of the maps corresponds to the finding that no statistically significant emissivity anomaly is found at 1.10 μm at present $N_r = 64$ -sensitivity. In contrast, the MST illustrated in Fig. A.6 shows a much better agreement between the fine-structures of the patterns, although the general appearances are not nearly as similar as for the analogous maps at 1.02 μm . The PMT depicted in Figs. A.6c and d contributes the largest SRMSD to the total error at 1.18 μm .

References

- DeGroot M. H. and Schervish M. J. *Probability and Statistics, Fourth Edition*. Addison-Wesley series in statistics. Addison-Wesley, 2012. ISBN 9780321500465.
- Hogben L. *Handbook of Linear Algebra*. Discrete Mathematics and Its Applications. CRC Press, 2006. ISBN 9781420010572.
- Kappel D., Arnold G., and Haus R. Multi-spectrum retrieval of Venus IR surface emissivity maps from VIRTIS/VEX nightside measurements at Themis Regio. *Icarus*, 265:42–62, 2016. doi:10.1016/j.icarus.2015.10.014.
- Kappel D., Arnold G., Haus R., Piccioni G., and Drossart P. Refinements in the data analysis of VIRTIS-M-IR Venus nightside spectra. *Adv. Space Res.*, 50(2):228–255, 2012. ISSN 0273-1177. doi:10.1016/j.asr.2012.03.029.
- Kappel D., Haus R., and Arnold G. Error analysis for retrieval of Venus' IR surface emissivity from VIRTIS/VEX measurements. *Planet. Space Sci.*, 113–114:49–65, 2015b. ISSN 0032-0633. doi:10.1016/j.pss.2015.01.014. SI:Exploration of Venus.
- Shao J. *Mathematical Statistics*. Springer Texts in Statistics. Springer, 2003. ISBN 9780387953823.

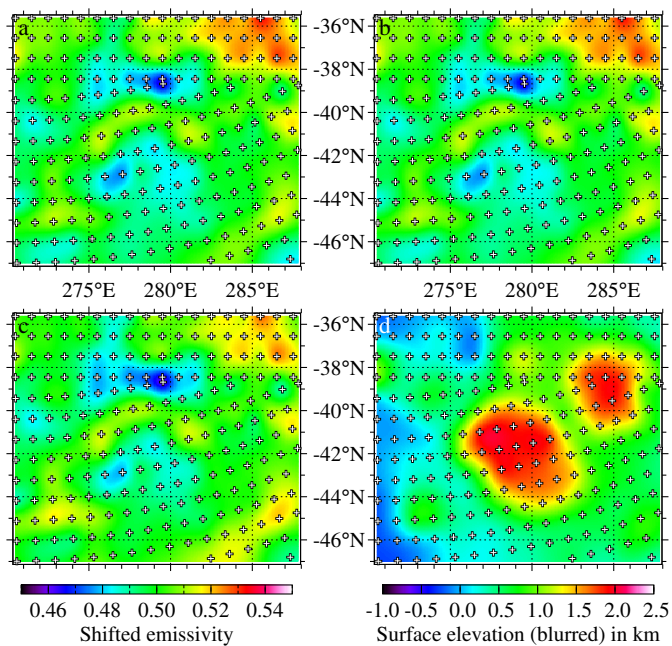


Figure A.4: Removal of trends with topography and latitude for the $1.18 \mu\text{m}$ emissivity map of Themis Regio retrieved from the $N_r^0 = 64$ measurement repetition data set. (a) Raw map, (b) trend with topography removed, (c) trends with topography and latitude removed, (d) utilized surface elevation (blurred Magellan topography). Representation as in Fig. 1.

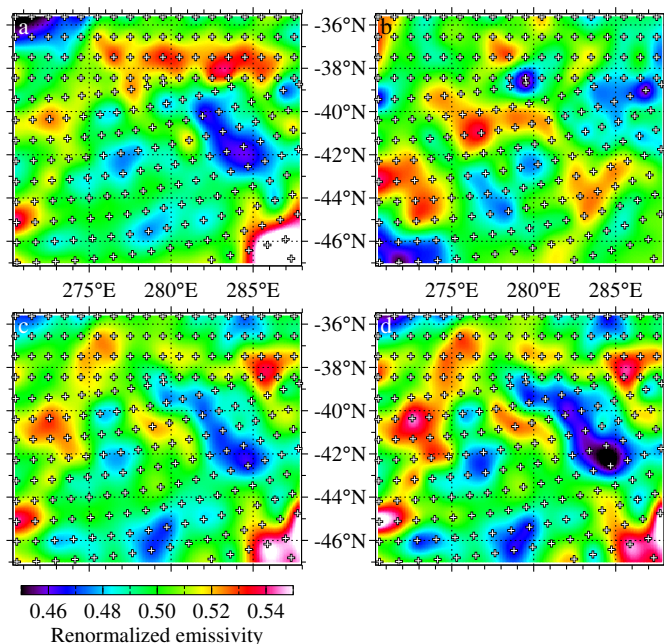


Figure A.5: Examples for MSTs and PMTs showing renormalized $1.10 \mu\text{m}$ emissivity maps of Themis Regio referred to reference emissivity 0.5. (a) MST 'N_r = 32, batch 1', (b) MST 'N_r = 32, batch 2', (c) PMT 'N_r = 25 base', (d) PMT 'Continuum 1.74 μm'. Representation as in Fig. 4.

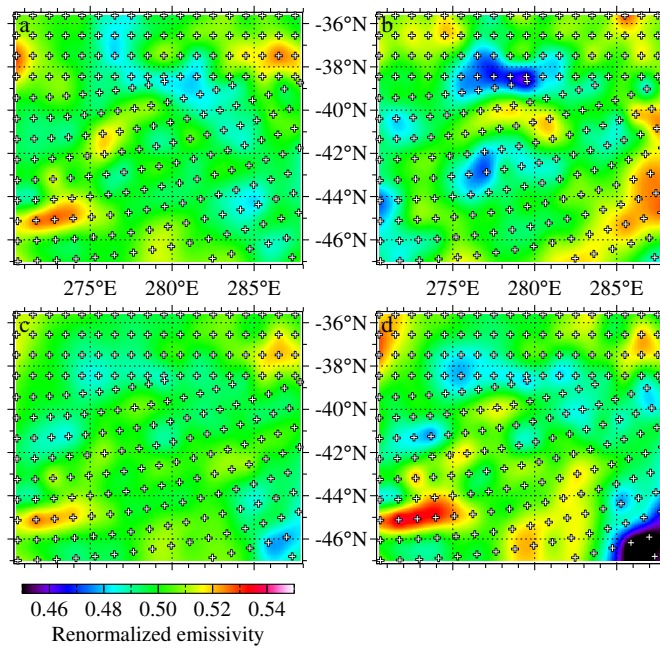


Figure A.6: Examples for MSTs and PMTs showing renormalized $1.18\ \mu\text{m}$ emissivity maps of Themis Regio referred to reference emissivity 0.5. (a) MST ' $N_r = 32$, batch 1', (b) MST ' $N_r = 32$, batch 2', (c) PMT ' $N_r = 25$ base', (d) PMT 'Continuum $1.74\ \mu\text{m}$ '. Representation as in Fig. 4.